ACS APPLIED MATERIALS & INTERFACES

Research Article

www.acsami.org

Construction of Hollow and Mesoporous ZnO Microsphere: A Facile Synthesis and Sensing Property

Jun Rao,[§] Ang Yu,[§] Changlin Shao, and Xingfu Zhou*

State Key Laboratory of Materials-Oriented Chemical Engineering, College of Chemistry and Chemical Engineering, Nanjing University of Technology, Nanjing 210009, P.R. China

Supporting Information

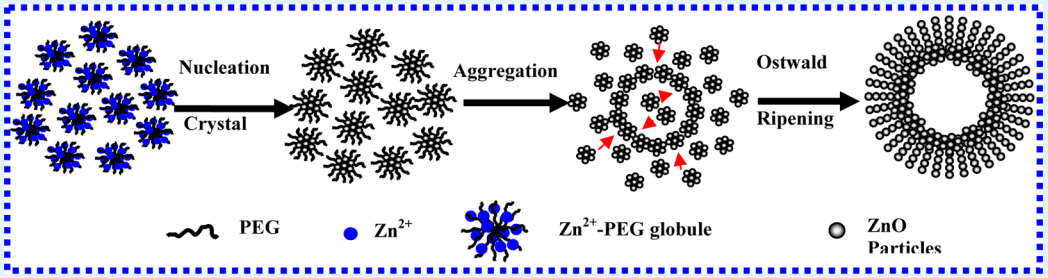

ABSTRACT: Mesoporous and hollow structure have been attracting increasing attention for their special properties and potential applications. Here we show a facile fabrication of hollow and mesoporous ZnO microsphere via a one-step wet chemical process using polyethylene glycol (PEG, MW 200) as the solvent and soft template. The morphology and structure of the products were characterized by using scanning electron microscopy and X-ray powder diffraction techniques. Thermal analysis and Fourier transform infrared spectroscopy techniques were also performed to show the properties of the precursor and annealed product. A possible growth mechanism of hollow and mesoporous ZnO microsphere was also proposed. The Brunauer−Emmett−Teller surface area of ZnO microsphere is 28.5 m^2g^{-1} and the size of mesopores is about 10 nm. The Photoluminescence spectra of the as-synthesized ZnO hollow microspheres were also presented. The mesoporous and hollow structure enhance the gas sensitivity of ZnO microsphere, and the obtained ZnO microspheres based sensor has an excellent performance for precision detection of ethanol and acetone with low concentration.

KEYWORDS: *mesoporous, ZnO, hollow microspheres, PEG 200, gas sensing*

INTRODUCTION

ZnO, an important metal-oxide semiconductor material with wide bandgap ($E_g \approx 3.7$ eV) and large exciton bonding energy (60 meV), can be used in numerous potential applications in optical device, solar cell, piezoelectric nanogenerator, gas sensor, and so forth.[1−5] Previous studies suggest that the morphology and size of materials have strong influence on their electrical and optical properties.[6] Different ZnO micro-nanostructures had been reported in recent years, such like nanowires, nanorods, nanotubes, nanosheets, hollow microspheres and some other novel structures.[7−12] Hollow spheres on microscale and nanoscale represent an important class of materials that has numerous advantages in the uses of optical and electrical properties and has attracted vast research interests.[13] Several kinds of strategies are utilized to construct and design hollow spheres, including Kirkendall effect, Ostwald ripening, and hard/soft templates. Railsback and co-workers have succeeded in the synthesis of hollow NiO spheres through the oxidation of Ni nanoparticles (NPs) via the nanoscale Kirkendall effect, this method can be extended to the synthesis of hollow microspheres of other semiconductor materials.[14] Zeng and co-workers devised an aqueous synthetic method to fabricate hollow nanospheres of Sn^{4+} doped anatase or rutile TiO_2 with high uniformity, study demonstrate that the Ostwald ripening mechanism is responsible for the creation of interior spaces of the oxide nanostructures.[15] Sano and co-workers utilized silica gels as the hard template to adsorb single-walled carbon nanotubes on silica gels and fabricate hollow spherical cage.[16] Yu and co-workers successfully synthesized CuS hollow nanospheres by using surfactant micelles as a soft-template.[17]

Mesoporous and hollow structure have been attracting increasing attention for their special properties and potential applications. However, it is difficult to fabricate mesoporous and hollow structure in a single process. Linear poly (ethylene glycol) (PEG) has been widely used as a template in the synthesis of a series of materials on microscale and nanoscale. Our research group has been interested in exploring the underlying connection of surfactant template, such as PEG, CTAB and oleic acid, with the structure and morphology of the micronanostructure materials.[8,10,18,19] Here we show in this paper a facile fabrication of mesoporous and hollow ZnO microsphere via a one-step wet chemical route using poly-

Received: July 11, 2012
Accepted: September 12, 2012
Published: September 12, 2012

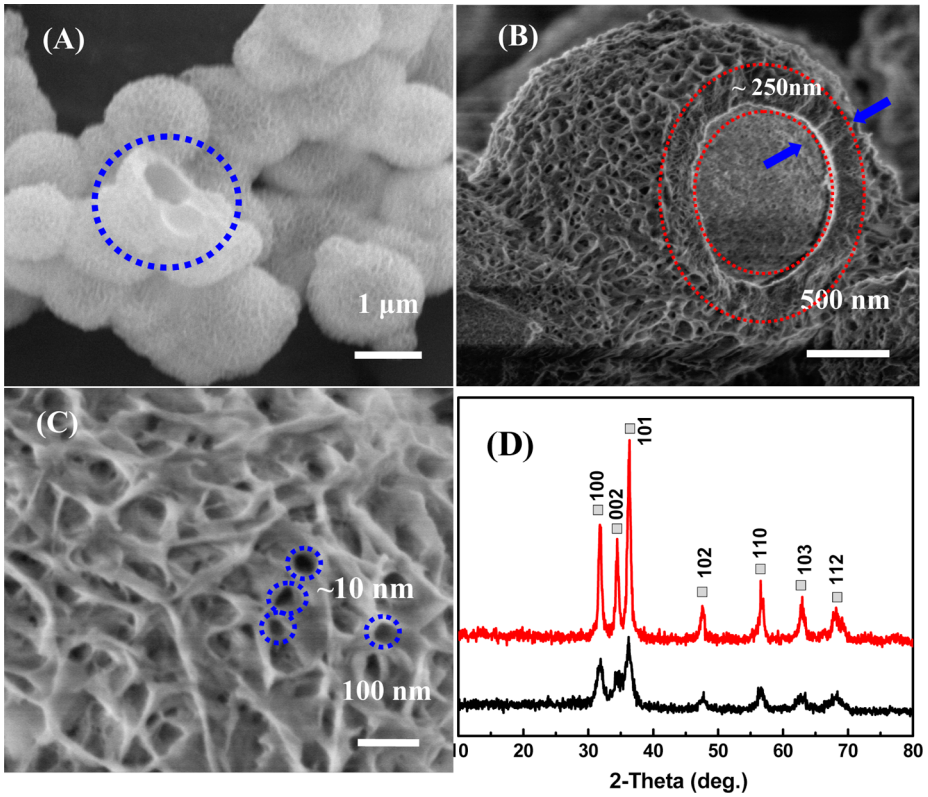

Figure 1. (A) SEM images of the as-synthesized ZnO hollow microspheres, circled area is a cracked ZnO microsphere. (B) FESEM image of an individual ZnO hollow microsphere. (C) Magnified FESEM image of the external surface of ZnO hollow microspheres. (D) XRD patterns of the precursor before annealing and sample after annealing.

ethylene glycol (PEG, MW 200) as the solvent and soft template, characterizations were preformed to reveal the growth mechanism of the as-synthesized ZnO hollow microspheres. The gas sensing property of ethanol and acetone with low concentration was also presented.

EXPERIMENTS

Mesoporous and hollow ZnO microspheres have been synthesized via a one-step reflux route. Typically, 10 mmol of zinc nitrate hexahydrate (2.973 g) was dissolved in 100 mL of polyethylene glycol 200 (PEG 200) under magnetically stirred and ultrasonic process, respectively. The mixed solution was then transferred into a 250 mL flask and gradually heated to 433 K. The refluxing process was kept for 6 h with magnetically stirring. After cooling down to room temperature, the brown powders were collected and washed with distilled water and absolute ethanol several times to remove the impurities. The brown powders were then annealing at 773 K for 4 h in a temperature-programmed Muffle furnace and the white powders were finally obtained.

The crystalline structure of samples were determined by the Bruker-D8 Advance X-ray diffractometer with graphite monochromatized high-intensity Cu Kα radiation at 40 KV and 30 mA, the data were collected at a scanning rate of 0.2 deg/s for 2θ value in the range of 10−80°. The morphology and size of the products were characterized by scanning electron microscopy (SEM, FEI Quanta-200), the fine structure of the material was obtained by a field emission scanning electron microscopy (FESEM, HITACHI S-4800). The transmission electron microscopy (TEM) and high-resolution transmission electron microscopy (HRTEM) observations were performed on a JEOL JEM-2010UHR instrument at an acceleration voltage of 200 kV. Thermal analysis (TG/DSC, STA409, Netzsch, Germany) was performed at a heating rate of 10 K/min under an oxygen atmosphere. Brunauer−Emmett−Teller (BET, Omnisorp100cx, and Coulter, U.S.A.) was measured to gain insight into the porous structure and distribution of the samples. Room-temperature photoluminescence (PL) spectra of the products were recorded on the Cary Eclipse EL0605−320328 spectrofluophotometer using the 328 nm Xe laser line as the excitation source.

ZnO sample powders were mixed separately with ethanol to make sticky pastes, which were then coated on the alumina tube-like substrate, on which gold electrode was preassembled. After dying the coated substrates in air, they were placed in the muffle furnace at 873K for 2 h. At last, a tiny Ni−Cr alloy coil was penetrated through the substrate tube to be a heater. The sensors were kept at working temperature for 120 h in order to improve the stability. The response tests were performed at the WS-30A gas sensing test system (Weisheng Electronics Co. Ltd., P.R. China). The gas response value is defined as S from the calculation of eq 1:

$$S = R_a/R_g \text{ (for reducing gas) or } S = R_g/R_a \text{ (for oxidizing gas)} \quad (1)$$

Where R_a and R_g are the sensor resistance in the air and testing gas environment, respectively.

RESULTS AND DISCUSSION

The morphology and structure of the mesoporous ZnO hollow microspheres were first characterized by SEM and XRD. The low magnified image in Figure 1A shows the overview of the uniform ZnO microspheres, it can be clearly observed that the ZnO microspheres have a uniform diameter of ~1.5 μm. The hollow structure can be judged by a cracked ZnO microsphere which is circled out in Figure 1A. Interestingly, the circled area clearly shows the cracked ZnO microsphere has a rough external surface and a smooth inner wall. The FESEM characterization of ZnO sample was further performed and a more intuitive microcosmic image is shown in images B and C in Figure 1. In Figure 1B, we can observe that a single cracked

dx.doi.org/10.1021/am3012966 | ACS Appl. Mater. Interfaces 2012, 4, 5346−5352

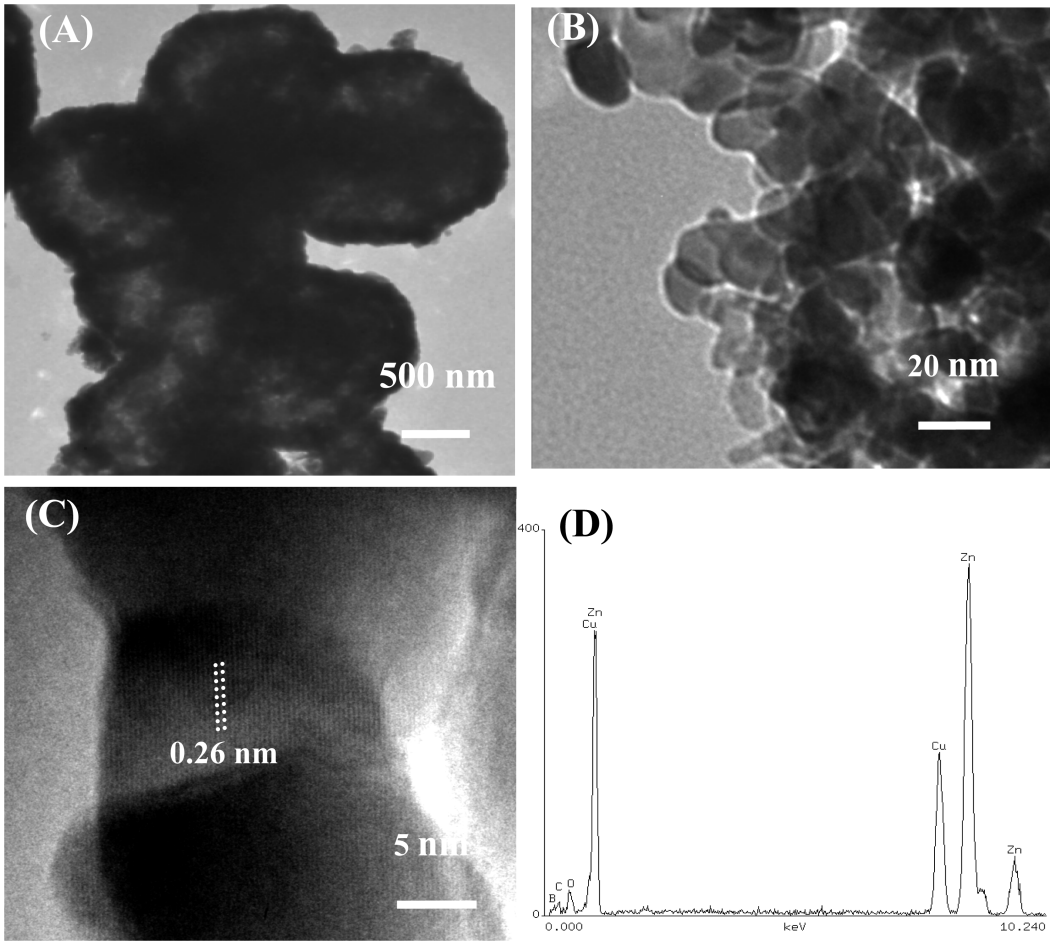

Figure 2. (A) TEM image of ZnO hollow microsphers. (B) HRTEM images of nano building blocks of ZnO hollow microsphere. (C) HRTEM lattice pattern of ZnO nanoparticles.(D) EDS of ZnO hollow microsphere.

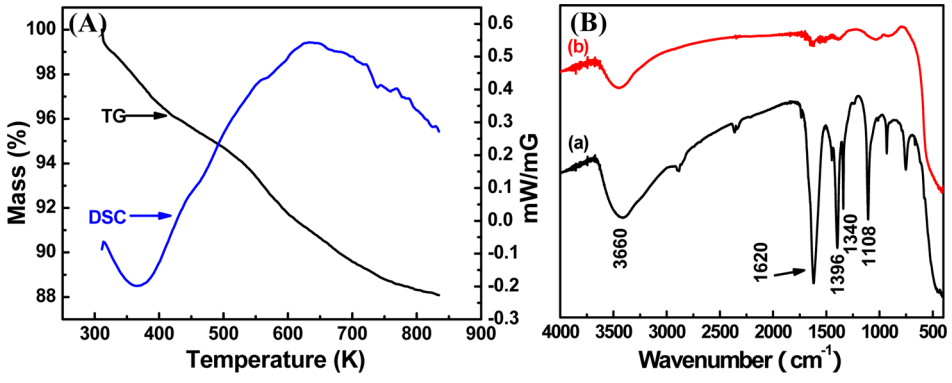

Figure 3. (A) TG-DSC plot of the precursor. (B) FTIR spectra of (a) the precursor and (b) ZnO obtained by calcination at 773 K.

hollow microsphere. The cracked hollow microsphere has a rough and porous external surface, and the porous structure in the smooth inner wall was also shown by carefully observation, which indicates that the pore in the external surface is larger than the pore in the inner wall. The thickness of ZnO hollow microspheres shell is about ~250 nm. We can find larger pores in the external surface, whereas smaller pores are in the inner wall, which indicates that the tapered pores penetrated the shell with its original larger holes in the external surface and the smaller terminal holes in the inner wall. A magnified image of the external surface was presented in Figure 1C. The diameter of porous structure is about 10 nm, which was marked in the Figure 1C. The phase compositions of the precursor before annealing and sample after annealing were examined by X-ray diffraction diffractometer and displayed in Figure 1D. Both diffraction patterns are indexing to the hexagonal ZnO with a wurtzite structure, and the lattice parameters of c and a of this hexagonal phase are 5.21 and 3.25 Å (P63mc, JCPDS Card No.36−1451), respectively. The stronger and sharper diffraction peaks of ZnO, which indicate to good crystalline, can be obtained after the precursor was annealed at 673 K for 2 h. The typic TEM, TEM and EDS image of ZnO hollow microspheres are presented in the Supporting Information, which further

dx.doi.org/10.1021/am3012966 | ACS Appl. Mater. Interfaces 2012, 4, 5346−5352

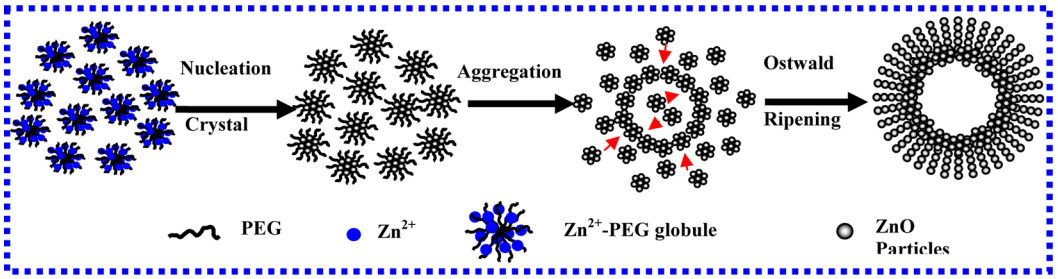

Figure 4. Schematic representation of the formation of ZnO hollow microsphere.

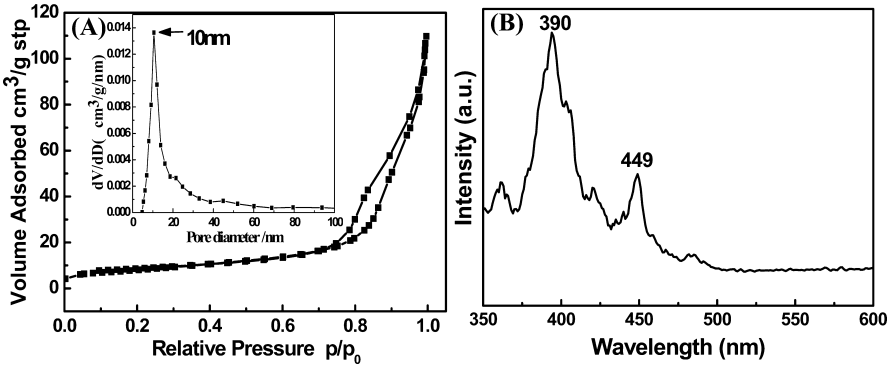

Figure 5. (A) Nitrogen adsorption/desorption isotherm and Barrett–Joyner–Halenda (BJH) pore size distribution plot (inset) of the as-synthesized ZnO hollow microspheres. (B) Photoluminescence spectra of the as-synthesized ZnO hollow microspheres.

interprets the hollow and mesoporous structures of ZnO microsphere.

The morphology and structure of the as-prepared ZnO microspheres architectures are further characterized by transmission electron microscopy (TEM) and high-resolution TEM (HRTEM) as shown in Figure 2. TEM images of the as-synthesized samples clearly show that the samples consist of ZnO spheres in the micrometer size range. The dark shell and pale center of the spheres suggests the hollow nature of the sample (Figure 2A). The shell thickness of the spheres is about 250 nm. High-resolution TEM (HRTEM) in Figure 2B observations reveal that the shell of hollow microsphere is constructed with ~20 nm ZnO nanoparticles. The clear lattice image indicates the good crystallinity and single crystalline nature of the ZnO nanoparticles. The HRTEM image of nano building blocks of ZnO hollow microsphere was shown in Figure 2C. The orderly and clear lattice fringes, parallel to each other, show that the building block of the microsphere are well-crystallized, and the interplanar distance between adjacent lattice planes is 0.26 nm, corresponding to the *d*-spacing value of ZnO (001) planes. The EDS analysis reveals the microsphere are composed of Zn and O elements (Figure 2D), which is consistent with the XRD result.

Thermal properties of the as-synthesized ZnO hollow microspheres were measured by thermogravimetic analysis and differential scanning calorimeter (TG/DSC). Test conditions were started from 313 to 873 K at a rate of 10 K/min in a flowing oxygen environment. The TG/DSC curves of the ZnO microspheres are shown in Figure 3A. It can be observed that the DSC plot presents the endothermic peak at 373 K and exothermic peak at 650 K, which corresponds to the evaporation of water and exothermic combustion of PEG 200, respectively. The weight loss distinctly occurs in the test range from 313 to 873 K, the weight loss is about 12%. Figure 3B shows the FT-IR spectrum of the ZnO precursor (a) and ZnO hollow microspheres after annealing at 773 K for 4 h (b). The majority of infrared absorption peaks are located in the middle and lower frequency zones. The curve (a) is the FT-IR spectrum of the ZnO precursor. The hydroxyl groups and water molecules are confirmed by the broad bands detected at high frequency at around 3660 cm^{-1}. The −CH− stretching band belonging to the PEG block appears between 2300 and 2830 cm^{-1}.[20] A sharp absorption at 1620 cm^{-1} in the higher frequency range is assigned to the O−H stretching from Zn−OH bonds.[21] The strong peaks at 1396 cm^{-1} correspond to the existence of PEG.[22] The intensive bands below 500 cm^{-1} are attributed to the vibrational modes of Zn−O.[23,24] IR spectra curve (b) of ZnO hollow microspheres after calcinations show that absorption peaks of organic groups are greatly weakened, indicating complete formation of ZnO hollow microspheres without organic groups.

On the basis of the results and discussions, a plausible formation mechanism of ZnO hollow microspheres is proposed and schematically illustrated in Figure 4. As a nonionic surfactant, PEG owns hydrophobic $-CH_2-CH_2-$ moieties and hydrophilic −O− on the long chain. Strong interaction between PEG chains and metallic species makes PEG chains wrapping with each other with zinc species in between, and this coordination interaction of PEG and metallic species had been proved to aggregate Zn^{2+}–PEG into globules.[8,18] The Zn^{2+}–PEG globules acts as the soft templates for the formation of ZnO hollow microspheres. In the initial of the reaction, Zn^{2+} ionic began to nucleate at the surface of Zn^{2+}–PEG globule with the increase of temperature. ZnO nanoparticles connect with each other at the surface of Zn^{2+}–PEG globule and form the initial ZnO microsphere.

Ostwald ripening process refers to the growth of larger crystals from those of smaller size which have a higher solubility than the larger ones. Previous studies had reported that Ostwald ripening occurred in the hydrothermal process.[10] In

dx.doi.org/10.1021/am3012966 | ACS Appl. Mater. Interfaces 2012, 4, 5346−5352

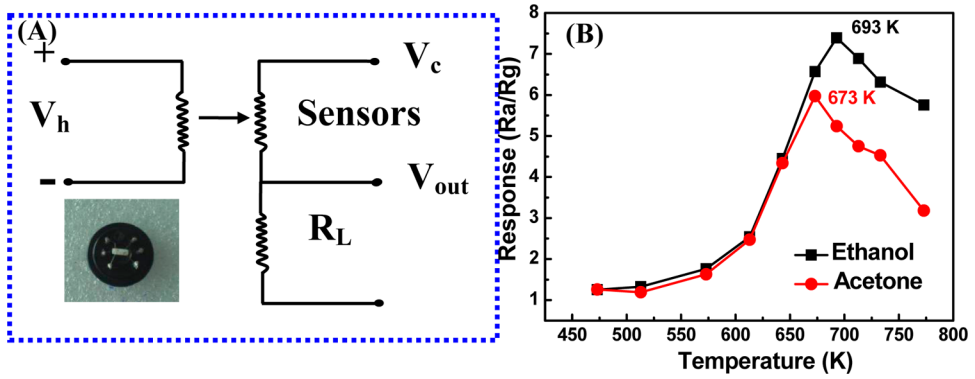

Figure 6. (A) Working principle of gas sensor test, down left is the photos of the practical sensor. (B) Gas sensing responses values of as-fabricated gas sensors with different working temperatures in 50 ppm ethanol and acetone, respectively.

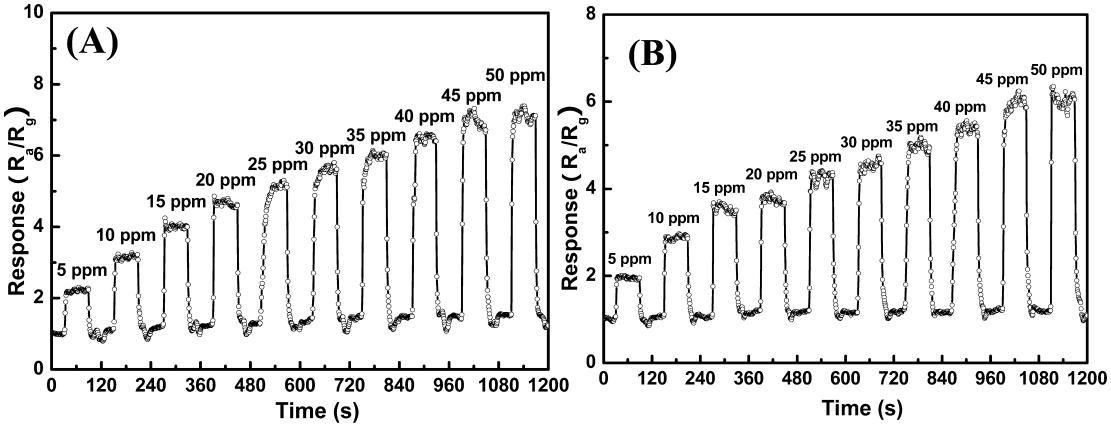

Figure 7. Gas response value curves of the ZnO hollow microspheres sensor to (A) ethanol and (B) acetone.

our experiment, the well-crystallized nanoparticles in external surface grow larger with the dissolution of weak-crystallized ones in the inner of the sphere, the dissolution of ZnO in the core lead to the formation of the hollow structure. Because of the nonuniform distribution of zinc ions, the concentration of zinc ions in Zn^{2+}−PEG globule is much larger than in the solution. The well-crystallized nanoparticles on the surface of the spherical shell grow larger with the dissolution of the neighboring weak-crystallized ZnO clusters, thus lead to the larger pores in the surface of ZnO microsphere. The smaller pores in the inner wall were formed with the complete dissolution of ZnO clusters in the core of the microsphere. The tapered pores penetrating the shell with its original larger holes in the external surface and the smaller terminal holes in the inner wall were finally formed during the Ostwald ripening process, which is consistent to the SEM results.

To obtain a further investigation on the porous structure and pore size distribution of the as-prepared sample, the Brunauer−Emmett−Teller (BET) measurement was performed to show the characteristic of the pores. As shown in Figure 5 A, the nitrogen physisorption isotherm exhibits a step increase in the volume of adsorbed nitrogen at a relative pressure of about 0.7 and the hysteresis in the high relative pressure range of 0.7−0.95 P/P_0, which belongs to type IV, indicating the existence of abundant mesoporous structures in the architectures according to IUPAC classification.[18] The BJH pore diameter distribution (inset in Figure 5A) shows a pronounced peak at ∼10 nm, confirming a high degree of uniformity of the pores, which is identical to the FESEM results. The specific BET surface area is 28.48 $m^2\ g^{-1}$ and the total pore volume is 0.15 $cm^3\ g^{-1}$.

The room-temperature photoluminescence (PL) spectra of the as-obtained hollow microspheres were recorded under UV excitations with an excitation wavelength of 328 nm. As shown in Figure 5B, the plot displays an intense UV emission at ∼390 nm, which came from the recombination of excitation centers in the ZnO crystal. The blue-green light emission at ∼449 nm attributed to the excitonic transitions with a band gap of 3.24 eV and a photo excited vacancy with the specific defect such as oxygen vacancies. No other peaks are observed. Previous studies showed that oxygen molecules would adsorb on the surface when the semicondor materials are exposed to air, the oxygen molecules would be formed as negative oxygen ions, such as O_2^-, O^-, and O^{2-}. The electrons are extracted from the conduction band and leads to a high resistance of semicondor materials in air. However, when the semicondor materials are exposed to reductive gases such as ethanol and acetone, the reductive gas will react with the oxygen species on the surface of ZnO, resulting in a decrease of ZnO resistance because the trapped electrons will be released back to the conduction band in this process. The existence of oxygen vacancies facilitates a high adsorption of oxygen, which increases the chance of ZnO interacting with reductive testing gases.[25] High specific surface area will also increase the percentage of surface atoms, which also contribute to the enhancement of the oxygen adsorption.[25,26]

The gas sensor properties of as-prepared sample with respect to the reductive gases such as ethanol and acetone were

dx.doi.org/10.1021/am3012966 | ACS Appl. Mater. Interfaces 2012, 4, 5346−5352

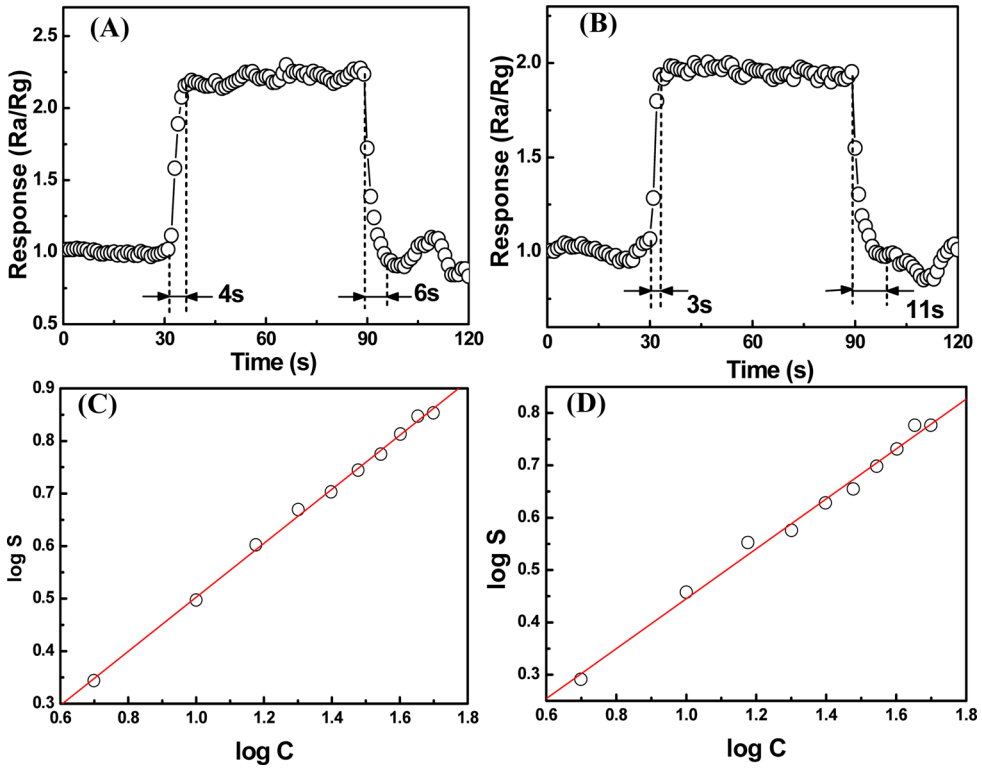

Figure 8. Response value curves of ZnO hollow microspheres in 5 ppm (A) ethanol and (B) acetone. (C) Logarithm plots of the ethanol sensor response value versus the concentration, (D) Logarithm plots of the acetone sensor response value versus the gas concentration.

measured at the WS-30A gas sensing test system. The sample was fabricated into three gas sensors for further measurements. Figure 6A shows the working principle of gas sensor test. A load resistance (R_L) is connected in series to the sensor. The sensor signal voltage (V_{out}) was collected by a computer at a test circuit voltage of 5 V (V_c). The down left image inset in Figure 6A is a picture of an as-fabricated gas sensor. Figure 6B shows the gas sensing responses values of as-fabricated gas sensors with different working temperatures in 50 ppm ethanol and acetone, respectively. The value of response signal is defined as the average value of S, as expressed in eq 1. It is obviously that the best working temperatures of gas sensors are 693 K for ethanol and 673 K for acetone, respectively.

Figure 7 is the gas sensing response curves of the sensors to ethanol and acetone with different concentrations, respectively. With the increasing test gas concentration from 5 ppm to 50 ppm, the responses values of gas sensor are obviously improving. The response value of sensor to 5 ppm ethanol is 2.2 (Figure 7A), which presents a higher response value than the carambola-like ZnO microspheres.[19] A similar result was observed for sensing acetone and shown in Figure 7B, the response values of ZnO are 2 in 5 ppm acetone. Moreover, the sensor was found to be stable during the experiment time and we did not observe the saturation phenomenon when the gas concentration was 50 ppm. It can be concluded that this sensor can be applied to detect ethanol and acetone with various low concentrations.

Panels A and B in Figure 8 show the response and recovery time of the ZnO hollow microspheres responding to ethanol and acetone. The response time is defined as the time needed for target gas to reach 90% of the equilibrium value, and the recovery time is the time needed for gas sensor to achieve a conductance 10% of the original value in air. The response and recovery time of the ZnO hollow microspheres in 5 ppm ethanol is 4 and 6 s (Figure 7A), whereas the response and recovery times are 3 and 11 s when exposed to 5 ppm acetone (Figure 7B).

An empirically representation of the gas response signal value of the semiconducting oxide sensor is

$$S = 1 + A_g(P_g)^{\beta} \quad (2)$$

Where P_g is the partial pressure of the testing gas, which is proportional to the gas concentration, A_g is a prefactor, and β is the exponent on P_g. Generally, the exponent β has an ideal value of either 0.5 or 1, which is derived from the surface interaction between chemisorbed oxygen and reductive gas to the n-type semiconductor.[27,28] The logarithm of the value calculated from eq 2 versus the logarithm of gas concentration is shown in C and D in Figure 8. The data can be fitted linearly very well and the slope of the fitting line is the correlation coefficient R of the ZnO hollow microspheres sensor. The correlation coefficient of ethanol sensor is 0.9989 at 693 K, and acetone sensor is 0.9958 at 673 K in the range from 5 to 50 ppm. The response and recovery time of the Fe-doped ZnO in 100 ppm ethanol is 6 and 5 s, and the response and recovery time is 3 and 8 s when exposed to acetone. The correlation coefficient of Fe-doped ZnO sensor to ethanol is 0.9974 and acetone sensor is 0.9957 in the range from 100 to 500 ppm at 673 K.[25] The sensitivities of these sensors fabricated by flowerlike, columnlike microcrystals ZnO/SnO_2 hierarchical nanostructures with a concentration of 10−1000 ppm are 209.8, 158.3, and 103.5, respectively. And the response time and the recovery time of the three samples are about 10 s.[29] Our hollow and mesoporous ZnO microsphere have an excellent performance for precision detection of ethanol and with low concentration (5−50 ppm). Such a fast response and

dx.doi.org/10.1021/am3012966 | ACS Appl. Mater. Interfaces 2012, 4, 5346−5352

recovery behavior could be explained by the structures of composite materials, such as mesoporous and hollow structures and large surface area, which easily enable analyte molecules to adsorb onto all the surfaces of materials.[30,31] These results show that the sensor matches with the dilogarithm amplifying circuits for precision detection and practical application in the detection range of 5−50 ppm of test gas. It is expected that hollow and mesoporous ZnO microsphere can be applied for monitoring ethanol and acetone vapor in the environment and food, or engineering test.[32]

CONCLUSION

In summary, mesoporous and hollow structured zinc oxide (ZnO) microspheres were successfully prepared by a facile one-step wet chemical route using polyethylene glycol (PEG, MW 200) as the solvent and soft template. Systematical investigation was performed to present the morphology, structure, gas sensing property and so on. Results indicate that the as-synthesized product was the mesoporous and hollow structures with BET surface area of 28.48 m^2 g^{-1} and the size of mesopores is ∼10 nm, which presented an excellent performance for precision detection in very low concentration of ethanol and acetone.

ASSOCIATED CONTENT

Supporting Information

The gas-sensing mechanism of ZnO-based sensors. This material is available free of charge via the Internet at http://pubs.acs.org.

AUTHOR INFORMATION

Corresponding Author

*E-mail: Zhouxf@njut.edu.cn. Tel: +86-25-83172270.Fax: +86-25-83172270.

Author Contributions

§These authors contributed equally to this work.

Notes

The authors declare no competing financial interest.

ACKNOWLEDGMENTS

This research was supported by the Natural Science Foundation of China (No. U1162108, 51272104); the National Basic Research Program (2009CB623403, 2009CB623406), the Natural Science Foundation of Jiangsu Province (11KJA150002; 10KJB150006), the Science & Technology Pillar Program of Jiangsu Province (BE2009679), and the Financial Foundation of State Key Laboratory of Materials-Oriented Chemical Engineering.

REFERENCES

(1) Klingshirn, C. *Phys. Status Solidi b* **2007**, *244*, 3027−3073.
(2) Yang, P. D.; Yan, H. Q.; Mao, S.; Russo, R.; Johnson, J.; Saykally, R.; Morris, N.; Pham, J.; He, R. R.; Choi, H. J. *Adv. Funct. Mater.* **2002**, *12*, 323−331.
(3) Law, M.; Greene, L. E.; Johnson, J. C.; Saykally, R.; Yang, P. D. *Nat. Mater.* **2005**, *4*, 455−459.
(4) Dai, Z. R.; Pan, Z. W.; Wang, Z. L. *Adv. Funct. Mater.* **2003**, *13*, 9−24.
(5) Wan, Q.; Li, Q. H.; Chen, Y. J.; Wang, T. H.; He, X. L.; Li, J. P.; Lin, C. L. *Appl. Phys. Lett.* **2004**, *84*, 3654−3656.
(6) Alivisatos, A. P. *Science* **1996**, *271*, 933−937.
(7) Huang, M. H.; Mao, S.; Feick, H.; Yan, H. Q.; Wu, Y. Y.; Kind, H.; Weber, E.; Russo, R.; Yang, P. D. *Science* **2001**, *292*, 1897−1899.
(8) Zhou, X. F.; Chen, S. Y.; Zhang, D. Y.; Guo, X. F.; Ding, W. P.; Chen, Y. *Langmuir* **2006**, *22*, 1383−1387.
(9) Li, Q. C.; Kumar, V.; Li, Y.; Zhang, H. T.; Marks, T. J.; Chang, R. P. H. *Chem. Mater.* **2005**, *17*, 1001−1006.
(10) Zhou, X. F.; Hu, Z. L.; Fan, Y. Q.; Chen, S.; Ding, W. P.; Xu, N. P. *J. Phys. Chem. C* **2008**, *112*, 11722−11728.
(11) Liu, B.; Zeng, H. C. *Chem. Mater.* **2007**, *19*, 5824−5826.
(12) Yu, Q. J.; Yu, C. L.; Fu, W. Y.; Yuan, M. X.; Guo, J.; Li, M. H.; Liu, S. K.; Zou, G. T.; Yang, H. B. *J. Phys. Chem. C* **2009**, *113*, 12016−12021.
(13) Deng, Z. W.; Chen, M.; Gu, G. X.; Wu, L. M. *J. Phys. Chem. B* **2008**, *112*, 16−22.
(14) Railsback, J. G.; Johnston-Peck, A. C.; Wang, J. W.; Tracy, J. B. *ACS Nano* **2010**, *4*, 1913−1920.
(15) Li, J.; Zeng, H. C. *J. Am. Chem. Soc.* **2007**, *129*, 15839−15847.
(16) Sano, M.; Kamino, A.; Okamura, J.; Shinkai, S. *Nano Lett.* **2002**, *2*, 531−533.
(17) Yu, X. L.; Cao, C. B.; Zhu, H. S.; Li, Q. H.; Liu, C. L.; Gong, Q. H. *Adv. Funct. Mater.* **2007**, *17*, 1397−1401.
(18) Cui, Y. M.; Liu, L.; Li, B.; Zhou, X. F.; Xu, N. P. *J. Phys. Chem. C* **2010**, *114*, 2434−2439.
(19) Li, B.; Liu, S. Q.; Liu, L.; Cui, Y. M.; Guo, X. F.; Zhou, X. F. *Chin. J. Inorg. Chem.* **2010**, *63*, 591−595.
(20) Rajeswari, Y. N.; Chandra, Bose A. *Appl. Phys. A: Mater. Sci. Process.* **2011**, *103*, 33−42.
(21) Thangaraja, A.; Savitha, V.; Jegatheesan, K. *Int. J. Nanotechnol. Appl.* **2010**, *4*, 31−38.
(22) Liufu, S. C.; Xiao, H. N.; Li, Y. P. *Powder Technol.* **2005**, *145*, 20−24.
(23) Hong, R. Y.; Qian, J. Z.; Cao, J. X. *Powder Technol.* **2006**, *163*, 160−168.
(24) Kwon, Y. J.; Kim, K. H.; Lim, C. S.; Shim, K. B. *J. Ceram. Proc. Res.* **2002**, *3*, 146−149.
(25) Yu, A.; Qian, J. S.; Pan, H.; Cui, Y. M.; Xu, M. G.; Tu, L.; Chai, Q. L.; Zhou, X. F. *Sens. Actuators, B: Chem.* **2011**, *158*, 9−16.
(26) Liao, L.; Lu, H. B.; Li, J. C.; He, H.; Wang, D. F.; Fu, D. J.; Liu, C.; Zhang, W. F. *J. Phys. Chem. C* **2007**, *111*, 1900−1903.
(27) Kim, I.; Rothschild, A.; Hyodo, T.; Tuller, H. L. *Nano Lett.* **2006**, *6*, 193−198.
(28) Scott, R. W. J.; Yang, S. M.; Chabanis, G.; Coombs, N.; Willams, D. E.; Ozin, G. A. *Adv. Mater.* **2001**, *13*, 1468−1472.
(29) Li, C. C.; Yin, X. M.; Li, Q. H. *CrystEngComm* **2011**, *13*, 1557−1563.
(30) Lee, J. H. *Sens. Actuators, B: Chem.* **2009**, *140*, 319−336.
(31) Kolmakov, A.; Moskovits, M. *Annu. Rev. Mater. Res.* **2004**, *34*, 151−180.
(32) Zhao, Y.; Jian,g, L. *Adv. Mater.* **2000**, *21*, 1−4.